Self-normalized photoacoustic techniques for thermal diffusivity measurements in metals

J. A. Balderas-López

Departamento de Matemáticas, Unidad Profesional Interdisciplinaria de Biotecnología del IPN,
Avenida Acueducto S/N, Col. Barrio la Laguna, Del. Gustavo A. Madero, C. P. 07340, México, D. F.México,
e-mail: abrahambalderas@hotmail.com and abalderas@acei.upibi.ipn.mx.

The analytical solution for the one-dimensional heat diffusion problem involving an harmonic heat source in a single layer, in the surface absorption limit, is used to provide self-normalized methodologies for thermal diffusivity measurements in metals, by using the photoacoustic technique. The self-normalized procedure involves the photoacoustic phase lag between the rear and front configurations. Three methodologies are described. Two of them involving linear fits in the photoacoustic thermally thin and thermally thick regimes. Comparison between the theoretical normalized equations and the corresponding normalized experimental data allows for the development of criteria on the selection of an appropriate modulation frequency range where a reliable analysis can be done. Computer simulations and thermal diffusivity values measured for some materials are also provided. The values of thermal diffusivity for each material, obtained by using the different reported methodologies, were found to be close to each other, showing self-consistency between the different methodologies described in this paper.

Keywords: Photoacoustic techniques; thermal diffusivity; metals.

Se utiliza la solución analítica para el problema de difusión de calor en una dimension, asumiendo una fuente de calor armónica en una capa, en el límite de absorción superficial, para el desarrollo de metodologías fotoacústicas normalizadas para medir difusividad térmica en metales. El procedimeinto de autonormalización involucra el retardo en la fase fotoacústica entre las configuraciones trasera y delantera. Se describen tres metodologías: dos de las cuales involucran ajustes lineales en los regímenes fotoacústicos térmicamente grueso y térmicamente fino. La correspondencia directa entre las ecuaciones teóricas y los datos experimentales permiten el desarrollo de criterios para la selección de los intervalos de frecuencia de modulación apropiados donde un análisis confiable puede llevarse a cabo. Se provee también con simulaciones por computadora y valores de difusividad térmica medidos para algunos materiales. Los valores de difusividad térmica, medidos utilizando las diferentes metodologías reportadas, se encontraron muy cercanos unos con otros, mostrando autoconsistencia entre las diferentes metodologías reportadas en este artículo.

Descriptores: Técnicas fotoacústicas; difusividad térmica; metales.

PACS: 07.20.Ym; 66.70.+f

1. Introduction

The Photoacoustic Techniques (PAT) have been extensively used for thermal diagnostics in a diversity of materials [1–6]. The basic principle of these techniques consists on the indirect measurement of the temperature fluctuations in a sample as a result of the nonradiative deexitacion process that takes place following the absorption of intensity modulated-radiation. With some few exceptions [6] PAT involve the analysis of the photothermal signal as a function of the modulation frequency. This brings, as a consequence, to the problem of transfer function determination. The transfer function is the modulation frequency response of the experimental system's electronics. If it is not provided an adequate procedure to take into account, or eliminate, this transfer function it is quit difficult to obtain reliable information about the properties to be measured by means of PAT. Data normalization is a very suitable procedure because, aside from the elimination of the transfer function, it reduce the number of parameters required for a quantitative analysis, thus increasing simplicity and realibility [7–9].

Although the application of PAT in metals involves a relatively simple mathematical model based on surface absorp-

tion, data analysis faces some dificulties, even though the transfer function is eliminated. At low modulation frequencies three-dimensional (3-D) effects may appear mainly due to the generally long thermal diffusion length in some metals owing to their large thermal diffusivity. At high modulation frequencies, the weak photothermal signal is highly influenced by other phenomena such as thermo-elastic contributions in the case of photoacoustic detection.

In this paper a self-normalization procedure is developed for measuring the thermal diffusivity of metals using a photoacoustic (PA) setup. This methodology is based on the signal ratio for front and rear surface experimental PA configurations and develops a set of reliable criteria verifying detection of purely thermal-diffusion -wave-generated PA signal within the entirely thermally thin or thermally thick limit. Three analytical procedures are provided, two of them involving linear fits in the PA thermally thin and thermally thick regimes. In the low modulation frequency range (thermally thin regime) the analytical procedure is based on the linear behavior of $\tan(\Phi)$ as a function of the modulation frequency, Φ been the phase lag difference between the rear and front PA configurations. On the other side, in the high modu-

lation frequency range (thermally thick regime), another analytical procedure based on the linear behavior of Φ, as a function of the root square of the modulation frequency, is provided. The direct comparison between the theoretical normalized equations and the normalized experimental data (no transfer function involved) allows for the development of criteria on the selection of an appropriate modulation frequency range where a reliable analysis can be done. In addition to the two fore mentioned methodologies another procedure, based on the theoretically predicted discontinuities in $\tan(\Phi)$, is provided for the direct measurement of the sample's thermal diffusivity. The presented methodologies were tested for two metals (commercial samples of copper and aluminum). The resulting thermal diffusivity values measured by using the different described methodologies were found close to each other, showing self-consistency between the different methodologies.

2. Theory

2.1. Mathematical model

Considering the one-dimensional heat diffusion problem for a single layer, with harmonic heat source, and assuming the surface absorption model, it is easy to shown that the temperature fluctuations on both surfaces of the material m (Fig. 1), are given by [7,9]

$$T_F(f,t) = \frac{I_0(\beta d)}{4k_m\sigma_m}(1+\gamma_{gm})\frac{(1+\gamma_{gm}e^{-2\sigma_m l})e^{i\omega t}}{(1-\gamma_{gm}^2 e^{-2\sigma_m l})},$$

$$\text{at } x = 0 \quad (1)$$

$$T_R(f,t) = \frac{I_0(\beta d)}{4k_m\sigma_m}(1+\gamma_{gm})^2\frac{e^{-\sigma_m l}e^{i\omega t}}{(1-\gamma_{gm}^2 e^{-2\sigma_m l})},$$

$$\text{at } x = -l \quad (2)$$

where I_0 is the light intensity impinging the surface of the material m, α_j, $j = m, g$, corresponds to the thermal diffusivity of medium j; (βd) is the absorbance of the infinitesimal layer of material m where total absorption of light takes place, and k_m is the corresponding thermal conductivity. σ_k, $k = g, m$, is the complex thermal diffusion coefficient, and γ_{gm} are the so-called thermal-wave reflection coefficients [9]. On considering PA techniques, it happens that the corresponding signals is proportional to the temperature fluctuations in the interfaces between the sample m and the medium g [10]. Taking the ratio T_R/T_F, it is clear that the proportionality factor, the transfer function and some other common constants in Eqs. (1) and (2) are eliminated and the following simpler expression is obtained:

$$R(f) = (1+\gamma_{gm})\frac{e^{-\sigma_m l}}{[1+\gamma_{gm}e^{-2\sigma_m l}]}. \quad (3)$$

For metals $\gamma_{gm} \cong 1$ and the ratio of amplitudes, $|R|$, and phase lag, Φ, of the complex signal $R(f)$ can be written as [7]
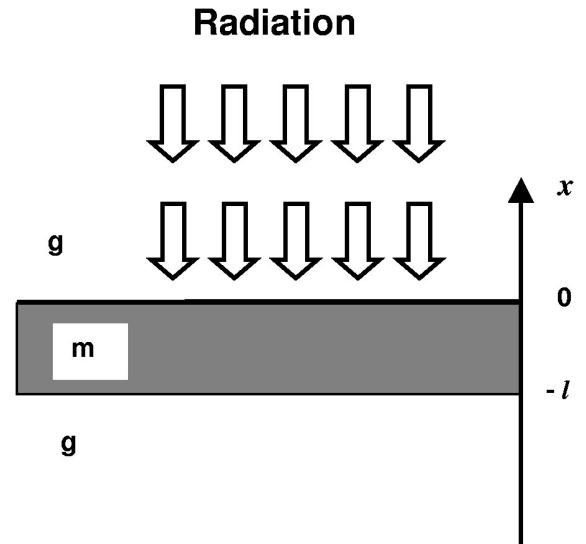
Radiation

FIGURE 1. Schematic representation of the one-dimensional single-layer photoacoustic model with surface absorption. g: gas (air); m: metal sample.

$$|R| = \frac{\sqrt{2}}{(\cosh(2x) + \cos(2x))^{1/2}}, \quad (4)$$

$$\tan(\Phi) = -\tanh(x)\tan(x) \quad (5)$$

where $x = (\pi f/\alpha_m)^{1/2}l$. In principle both of these two equations can be used for thermal diffusivity purposes in metals, however, as it was pointed out before, the lack of criteria to chose an adequate modulation frequency range, in which a confident analysis can be done, makes the corresponding analytical procedure highly uncertain. This is especially true for the ratio of PA amplitudes (Eq. (4)), which is highly sensitive to light source fluctuations and surface's reflectivity. The PA phase lag, Φ, results more suitable for analytical purposes because it does not share such complications. Even more it is possible to derive simple expressions for Φ and $\tan(\Phi)$ in the high and low modulation frequency regime, respectively, for the matter of evaluation of the sample's thermal diffusivity. In the low modulation frequency regime, this can be done by considering the series expansion for the functions $\tanh(x)$ and $\tan(x)$ in Eq. (5) [11]. By keeping only linear terms in both series it is easy to shown that

$$\tan(\Phi) = -x^2 = -\left[\frac{\pi}{\alpha_m}l^2\right]f. \quad (6)$$

Equation (6) shows that a linear relation for $\tan(\Phi)$, as a function of the modulation frequency, must to be obtained at low modulation frequencies. An analytical procedure based on Eq. (6) involves the fit of $\tan(\Phi)$ vs f (the modulation frequency), in the low modulation frequency range. The sample's thermal diffusivity can be obtained by means of the fitting parameter $M = \pi l^2/\alpha_m$.

On the other hand, in the high modulation frequency regime the asymptotic behavior for Φ can be considered instead. From Eq. (5) it is easy to shown that if $x \gg 1$ then

$$\Phi = -x = -\left(\sqrt{\frac{\pi}{\alpha_m}}l\right)\sqrt{f} \qquad (7)$$

This equation shows that the phase behaves asymptotically as $f^{1/2}$. The corresponding analytical procedure based on Eq. (7) involves the fit of the experimental PA difference of phases, Φ, as a function of the root square of the modulation frequency, in the range of high modulation frequencies. The sample's thermal diffusivity can be obtained from the fitting parameter $P = (\pi/\alpha_m)^{1/2}l$. Because Eqs. (3) to (7) where obtained eliminating the experimental transfer function in the process, any theoretical predictions from them must directly match to the corresponding experimental results. In particular Eq. (5) predicts that if $x = 0$ ($f = 0$) then $\tan(\Phi) = 0$, this requirement can be taken as a criteria for to chose an adequate modulation frequency range, in the low and high modulation frequency regimes, where experimental data sub-sets can be selected for a confident analysis, as it will shown later. Close analysis of Eq. (5) shows the existence of discontinuities on $\tan(\Phi)$ on values for x given by $x = (2n+1)\pi/2$. This fact suggests the possibility for measuring the sample's thermal diffusivity by the direct localization of these discontinuities. The analytical procedure involves the plotting of $\tan(\Phi)$, as a function of the modulation frequency, and the localization of the modulation frequencies values where these discontinuities are taking place. Although it depends on the material, usually only the first discontinuity will be experimentally reached. For this first discontinuity $n = 0$ and the sample's thermal diffusivity can be evaluated as

$$\alpha_m = \frac{4f_1 l^2}{\pi}, \qquad (8)$$

where f_1 is the value of modulation frequency where the first discontinuity takes place. The corresponding thermal diffusivity can be obtained by means of the Eq. (8), once this value of modulation frequency is known.

2.2. Computer simulations

To illustrate the general aspects of the theoretical 1-D model to be compared with the experimental results some computer simulations are provided (Figs. 2 to 5). These simulations were done making use of Eq. (3), assuming two different values for l and the thermal properties reported in the literature for pure aluminum and copper (Table I). Figure 2 shows the theoretical ratio of PA amplitudes (Eq. (4)) as a function of the modulation frequency. As it is evident from this figure, the ideal 1-D model predicts a flat region on the plot of this variable in the very low modulation frequency regime, corresponding to the extremely thermally thin behavior of the PA signal ($\exp(-\sigma_m l) \cong 1$). In this regime the theoretical ratio of PA amplitudes is equal to one. As larger is the value of thermal diffusivity, as wider is the extent of this flat region.

The opposite is true when the sample's thickness is considered instead (thicker samples show narrower extension on the flat region), as predicted from Eq. (3) and observed in Fig. 2. Because at these very low modulation frequency values 3-D effects could be experimentally observed, the analysis of the experimental ratio of amplitudes and its comparison with the corresponding theoretical predictions could be useful into the definition of the lower limit for the range of modulation frequencies on which experimental data could be chosen for the analysis in the thermally thin regime, as it will be shown later. Figure 3 shows the theoretical 1-D behavior of $\tan(\Phi)$, as a function of the modulation frequency, in the low modulation frequency regime. The linear dependence of this function, as predicted by Eq. (6), is evident in this low modulation frequency regime (continuous lines). These continuous lines were drawn evaluating the slopes $M = \pi l^2/\alpha_m$, by using the values for l and α_m in Table I, and demanding these lines intersect the origin of coordinates. As evident from this figure, the upper limit for the modulation frequency range, where this linear behavior takes place, is inverse related to the sample's thickness for a given material: as smaller the sample's thickness is, as larger is this upper limiting value. The opposite is true if the thickness is keep constant and the thermal diffusivity changes: as larger the thermal diffusivity is, as wider is the modulation frequency range where the linear behavior is obtained. The corresponding theoretical 1-D behavior for Φ, as a function of the modulation frequency root square, is shown in Fig. 4. The linear behavior, as predicted by Eq. (7), is evident in the high modulation frequency regime. The continuous lines on this figure were drawn by calculating the theoretical value for the slope $P = (\pi/\alpha_m)^{1/2}l$, for the given values of α_m and l (Table I), and demanding, as before, the intersection of these lines on the origin of coordinates. Because in the high modulation frequency domain the coupling between the purely PA thermal diffusion mechanism and thermo-elastic contributions difficult the analysis, the overlapping of this straight line on the plot for the experimental data and its requirement of intersecting the origin of coordinates could be a very important criterion on to decide on an adequate modulating frequency range for the analysis, by means of Eq. (7). The lower limit value for $f^{1/2}$, where the linear behavior takes place, is inversed related with the sample's thickness (for a given thermal diffusivity value) and directly related with the thermal diffusivity (for a constant thickness), as could be expected. Figure 5 shows the $\tan(\Phi)$ as a function of the modulation

TABLE I. Samples' thickness and thermal properties values, reported in the literature, for the materials used for computer simulations by means of Eq. (3).

Material	Thickness (cm)	k **W/cmK**	α
Aluminum (Pure)	$l_1 = 0.0300$	2.37	0.98
	$l_2 = 0.0500$	Ref. 12	Ref. 13
Copper (Pure)	$l_1 = 0.0300$	3.98	1.31
	$l_2 = 0.0500$	Ref. 12	Ref. 13

frequency, in an extended range, for the values of l and α_m as given in Table I. Due to the large thermal diffusivity values and the relatively small thickness values, assumed for the simulations, only the first discontinuity was obtained for three of the plots. The modulation frequency values, where these discontinuities take place, are in agreement with the modulation frequency values predicted from Eq. (8).
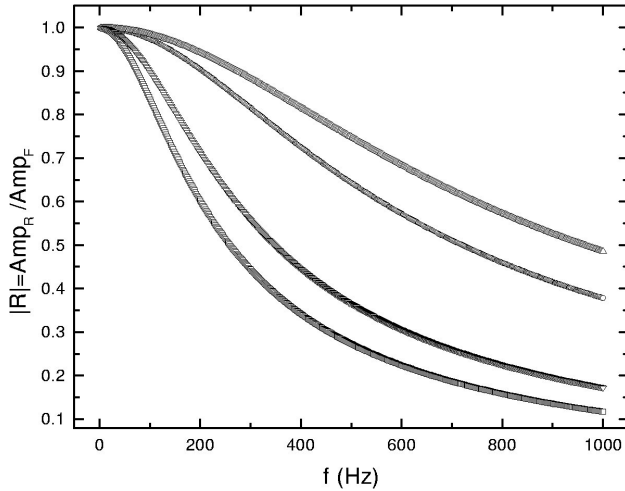

FIGURE 2. Computer simulation for $|R(f)|$ (ratio of amplitudes), for the different materials and their thickness (Table I), taken for the analysis. The correspondence curve-symbols is as follows: Circles ($\circ$) and squares ($\square$) for pure aluminum, thickness 0.03 cm and 0.05 cm, respectively; Triangle up ($\triangle$) and triangle down (∇) for pure copper, thickness 0.03 cm and 0.05 cm, respectively.
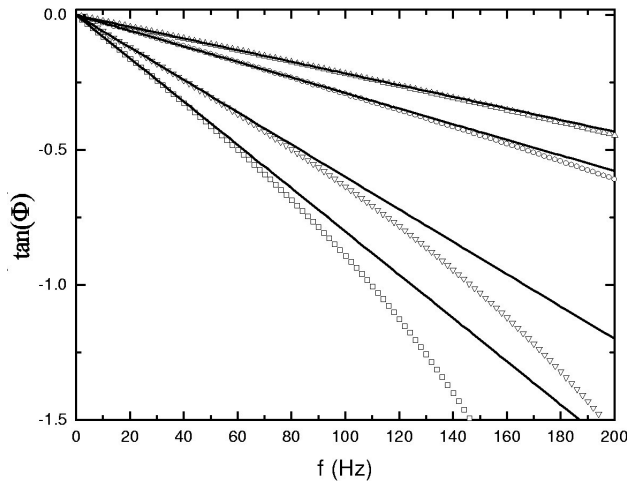

FIGURE 3. Computer simulation for $Tan(\Phi)$, as a function of the modulation frequency, for the different materials and their thickness (Table I), taken for the analysis, in the low modulation frequency range. The correspondence curve-symbol is as follows: Circles ($\circ$) and squares ($\square$) for pure aluminum, thickness 0.03 cm and 0.05 cm, respectively; Triangle up ($\triangle$) and triangle down (∇) for pure copper, thickness 0.03 cm and 0.05 cm, respectively.
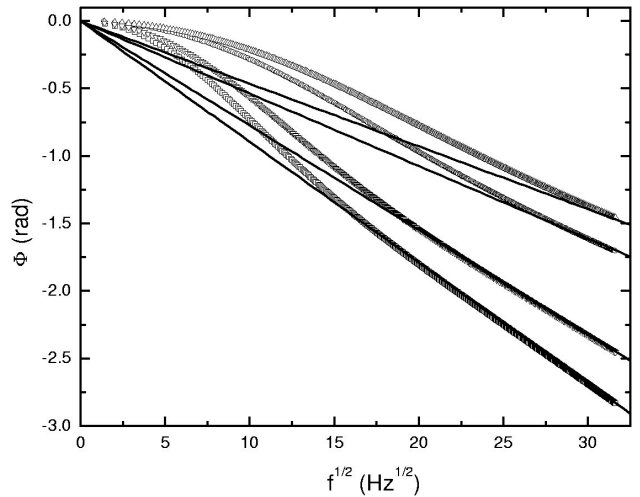

FIGURE 4. Computer simulation for the phase, Φ, as a function of the modulation frequency root square, for the different materials and their thickness (Table I), taken for the analysis. The correspondence curve-symbols is as follows: Circles ($\circ$) and squares ($\square$) for pure aluminum, thickness 0.03 cm and 0.05 cm, respectively; Triangle up ($\triangle$) and triangle down (∇) for pure copper, thickness 0.03 cm and 0.05 cm, respectively.
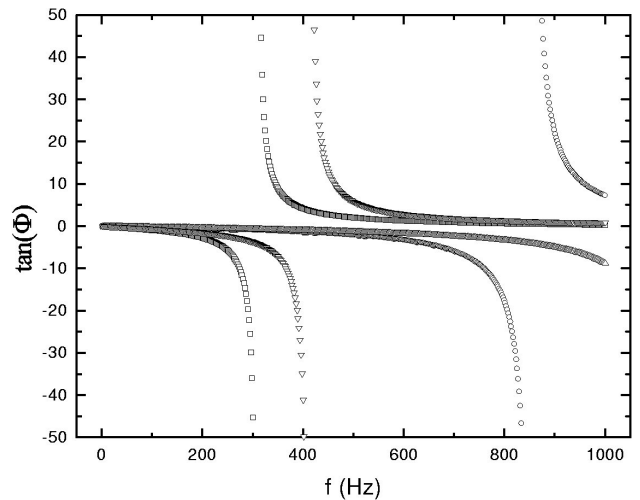

FIGURE 5. Computer simulation for $Tan(\Phi)$, as a function of the modulation frequency, for the different materials and their thickness (Table I), taken for the analysis. The correspondence curve-symbols is as follows: Circles ($\circ$) and squares ($\square$) for pure aluminum, thickness 0.03 cm and 0.05 cm, respectively; Triangle up ($\triangle$) and triangle down (∇) for pure copper, thickness 0.03 cm and 0.05 cm, respectively.

3. Experimental

The experimental PA set-up, shown in Fig. 6, consisted of an argon-ion laser (approximately 1 mm beam diameter), delivering 200 mW of dc power, whose beam was modulated by using an acousto-optic modulator. The PA cell consisted of a cylindrical hole (3 mm diameter and 3 mm length), made in a brass body and communicating with an electret microphone (with a built-in pre-amplifier) through a channel. The

PA chamber was obtained by placing the metallic sample (using vacuum grace) on the upper surface of the PA cell, and was sealed by using a thin plate (160 microns) of corning glass on the opposite side, working also as a window. To obtain the two PA configurations the modulated laser beam was sent to a beam splitter. The signal for the rear PA configuration was obtained by obstructing beam number one by means of an obstacle (Fig. 6), allowing, at this way, that only the beam number two impinges the upper surface of the sample. In a similar way the front PA configuration was obtained by obstructing, this time, beam number two. PA signals for both configurations were generated as a function of the modulation frequency in a range of 2 to 500 Hz, step 2 Hz, and then fed to a lock-in amplifier (SR, Model 830) for further amplification and demodulation. Two metal samples were used for this work (Table II): commercial copper and commercial aluminum slabs (originally at 2 mm and 4 mm thickness, respectively). Small pieces of these two samples were cut and polished to obtain thin layers of 440 microns (for copper) and 300 microns (for aluminum), as measured with the help of a micrometer calibrator (Mitutoyo, 5 microns precision).

4. Results and discussion

Figure 7 shows the experimental ratio of amplitudes, as a function of the modulation frequency, for the two samples. As it was expected, 3-D effects were observed. These 3-D effects are evident in Fig. 7 by looking on the non-flat region, in the very low modulation frequency regime (compare with Fig. 2), and were upper-delimiting by the vertical lines on the same figure (compare Fig. 2 with Fig. 7). In Figs. 8a
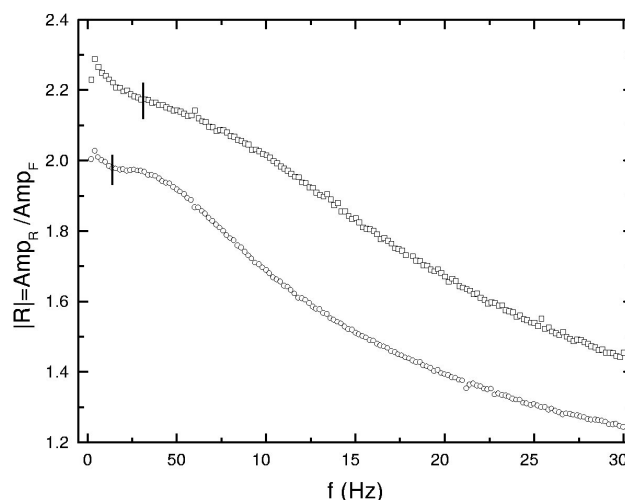

FIGURE 7. Ratio of amplitudes, $|R(f)|$, for the experimental PA signals in the rear and front configurations. Circles (○) correspond to a commercial aluminum sample (0.03 cm thickness) and Squares (□) correspond to a commercial copper sample (0.044 cm).

and 8b the corresponding experimental results for $\tan(\Phi)$, in the low modulation frequency regime, are shown. The lower limits for the modulation frequency ranges, to take data for the analysis by means of Eq. (8), were selected as the values marked by the vertical lines in Fig. (7). The corresponding upper limits were defined by overlapping straight lines on the plots of the experimental data and demanding these lines cross the origin of coordinates. These upper limits where selected on the modulation frequency values were the departure from the straight lines was evident. The continuous lines in these figures represent the best fits to Eq. (8) on the selected data subsets. The results are summarized in Table II (column 3). On the other hand, Figs. 9a) and 9b) show the experimental behavior for the phase lag, Φ, as a function of the modulation frequency root square. The linear behavior, this time at high modulation frequencies, as predicted by Eq. (7), is evident on these figures. The experimental data sub-sets chosen for analysis by means of this equation were selected by overlapping straight lines (dashed lines in the figures) to the corresponding plots and demands these lines intersect the origin of coordinates. The onset of the data sub-sets took for the analysis by means of Eq. (7) were marked by the vertical lines on the same plots. The continuous lines represent the best fits to Eq. (7) on those regions. The corresponding results are summarized in Table II (column 4). Finally Figs. 10 a) and 10 b) show $\tan(\Phi)$, as a function of the modulation frequency, for matter of localization of the values of modulation frequencies where, according to the Eqs. (5) and (8), the discontinuities take place. On the same plots the corresponding modulation frequency values, 1 Hz precision, are printed. Based on these values and the samples' thickness (Table II, column 2), the corresponding values for thermal diffusivity were calculated by means of the Eq. (8). These values are shown in Table II (column 5).
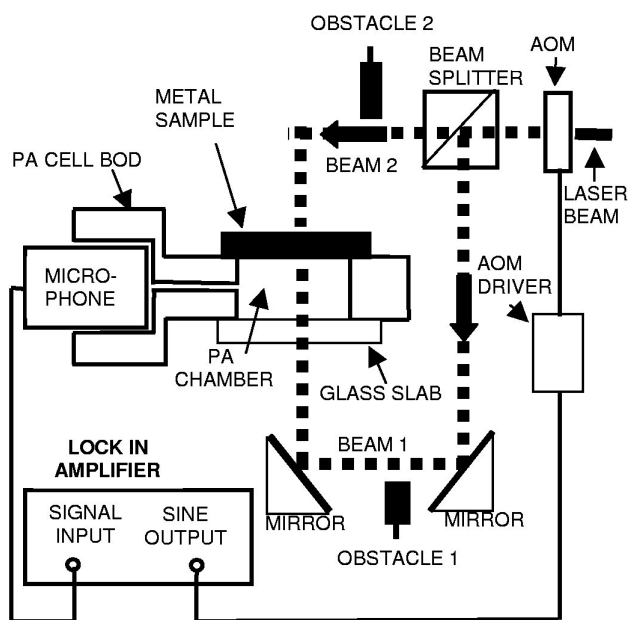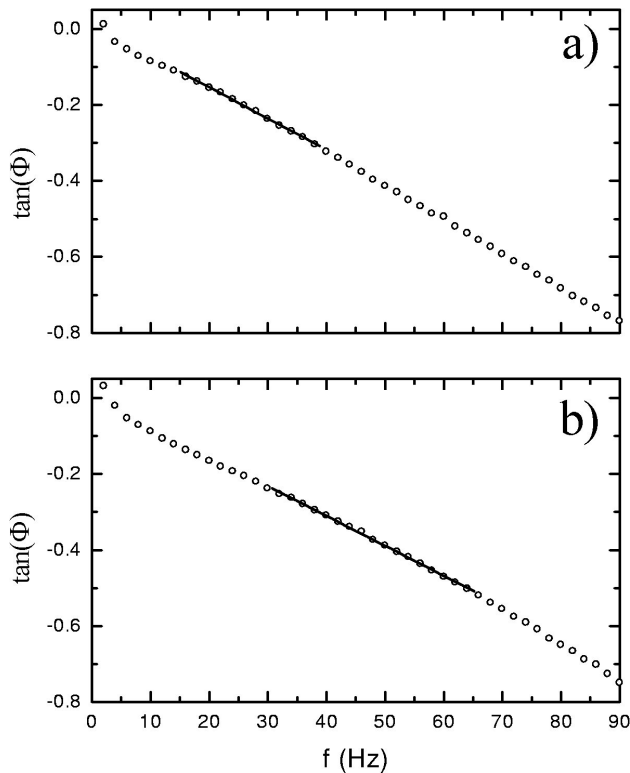

FIGURE 6. Schematic cross section of the photoacoustic (PA) configuration experimental setup used for the thermal diffusivity measurements. AOM: Acusto-Optic Modulator. An argon-ion laser was used as light source.

FIGURE 8. $\tan(\Phi)$ for the experimental difference of PA phase signals, Φ, in the rear and front configurations, in the low modulation frequency regime. a) commercial aluminum sample, b) commercial cupper sample. The continuous straight lines correspond to the best fits to Eq. (6).

TABLE II. Samples' thickness and the corresponding thermal diffusivity values obtained by using the different photoacoustic methodologies reported in this paper. α_{Thin} refers to the thermal diffusivity measured by using the linear fits for $\tan(\Phi)$, as a function of the modulation frequency, in the thermally thin regime; α_{Thick} refers to the thermal diffusivity measured by using the linear fits for Φ, as a function of the modulation frequency root square, in the thermally thick regime; α_{disc} refers to the thermal diffusivity measured by using the discontinuities for $\tan(\Phi)$.

Material	Thickness (cm)	α_{Thin} cm^2/s	α_{Thick} cm^2/s	α_{disc} cm^2/s
Aluminum (Commercial)	$l = 0.0300$	0.36	0.38	0.39
Copper (Commercial)	$l = 0.0440$	0.77	0.74	0.73

As it is evident from Table II (columns three to five), there is a remarkable agreement among the different thermal diffusivity values measured by using the different methodologies. Although these measured values are very different (almost a half) of the corresponding ones reported for the pure metals (Table I), these differences could be attached to the utilization of commercial samples for this study, moreover the process of polishing could bring, as a consequence, to a further diminution in the thermal properties for the materials.
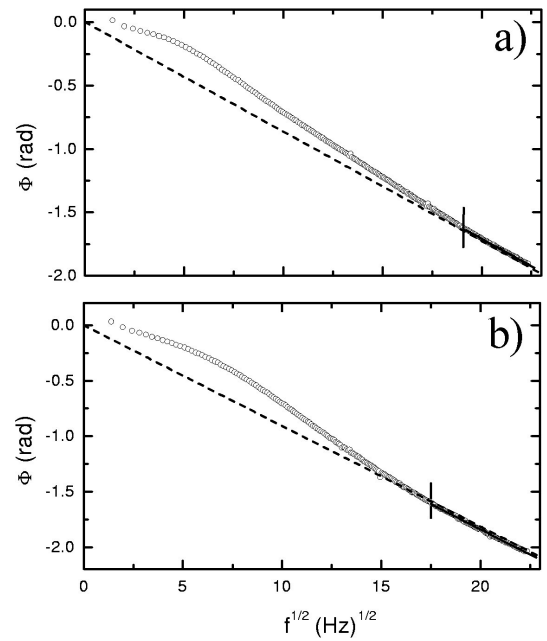

FIGURE 9. Difference of the experimental PA phases, Φ, in the rear and front configurations, in the high modulation frequency regime. a) commercial aluminum sample, b) commercial cupper sample. The continuous straight lines correspond to the best fits to Eq. (7). The dashed lines, draw on the same figures, were used for the selection of the best data subset in the high modulation frequency regime (the onset marked by the vertical lines) for the analysis, as described.
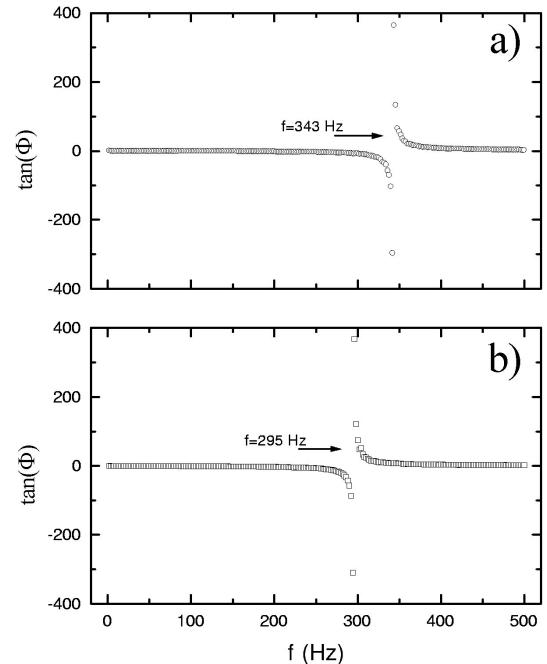

FIGURE 10. Tangent for the experimental difference of PA phase signals, Φ, in the rear and front PA configurations, as a function of the modulation frequency. a) commercial aluminum sample, b) commercial copper sample. The discontinuities on $\tan(\Phi)$, as predicted by Eq. (5), are evident in the plots. The corresponding modulation frequency values, where these discontinuities took place, printed in the plots, were used for thermal diffusivity measurements by means of Eq. (8).

5. Conclusions

In conclusion a self-normalized PA technique involving the rear and front PA signal phases has been presented for to make measurements of thermal diffusivity for metals. Because the signals for both PA configurations were obtained without moving the sample, the normalization procedure eliminates, in efficient way, the transfer function. The pre-dicted asymptotic value: $\tan(\Phi) = 0$ for $f = 0$, was rigorously applied and constitute a very useful criteria for choosing the adequate modulation frequency ranges where confident analysis, by means of Eqs. (6) and (7) can be made. In principle the PA methodologies reported in this paper could be applied to any opaque material, provided the theoretical conditions of the model are fulfilled. But, as it stands, these methodologies are especially suitable to metals.

1. A.C. Tam, *Rev. Mod. Phys*, **58** (1986) 381.

2. *Progress in Photothermal and Photoacoustic Science and Technology*, edited by A. Mandelis (Elsevier, New York, 1992), Vol. 1.

3. G. Rousset and F. Lepoutre, *J. Appl. Phys.* **54** (1983) 2383.

4. L.F. Perondi and L.C.M.Miranda, *J. Appl. Phys.* **62** (1987) 2955.

5. J.A. Balderas-López *et al.*, *Forest. Prod. J.* **46** (1986) 84.

6. J.A. Balderas-López and A. Mandelis, *Int. J. Thermophys.* **23** (2002) 605.

7. O. Pessoa, Jr. *et al.*, *J. Appl. Phys.* **59** (1986) 1316.

8. J.A. Balderas-López, G. Gutiérrez-Juárez, M.R. Jaime-Fonseca and F. Sánchez-Sinencio, *Rev. Sci. Instrum.* **70** (1999) 2069.

9. J.A. Balderas-López and A. Mandelis, *J. Appl. Phys.* **90** (2001) 2273.

10. A. Roscenwaig and A. Gersho, *J. Appl. Phys.* **47** (1976) 64.

11. *Mathematical handbook*, Murray R. Spiegel, Schaum's outlines. 35th Printing Mc Graw-Hill, 1996.

12. Y.S. Touloukian, R.W. Powell, C.Y. Ho, and M.C. Nicolau, *Thermal Conductivity for Metals* (IFI Plenum, New York, 1987).

13. Y.S. Touloukian, R.W. Powell, C.Y. Ho, and M.C. Nicolau, *Thermal Diffusivity* (IFI Plenum, New York, 1987).